ForensicSAR approach for detecting precursor deformation prior to the collapse of Derna Dam in Libya

Arliandy Pratama[1,2*], Wataru Takeuchi[2]
[1]Dept. of Civil Engineering, The University of Tokyo, Tokyo, Japan
[2]Institute of Industrial Science, The University of Tokyo, Tokyo, Japan
*arliandyarbad@g.ecc.u-tokyo.ac.jp

Abstract

On 10–11 September 2023, Storm Daniel triggered cascading failures of the Bu Mansour (Upper Derna) and Al-Bilad (Lower Derna) dams in Libya. We develop ForensicSAR, a workflow that densifies on-structure InSAR sampling and couples satellite-derived deformation metrics with lightweight finite-element (FEM) hypothesis testing. Dual-orbit Sentinel-1 time series (2019–2024) are decomposed into vertical (U) and east–west (E) components, and Tracy–Widom PS selection (TW-PSI) recovers ~40% more persistent scatterers over low-coherence dam bodies relative to ADI-PSI, stabilizing pre-event velocity, acceleration, and Δslope estimates. Within a 12-month pre-event window, we detect a localized precursor at Bu Mansour, concentrated over the crest and eastern sectors with elevated |Δslope| and zscores, whereas Al-Bilad shows weaker or inconsistent signals. Preliminary 2D Mohr–Coulomb FEM sections reproduce crest settlement and core-face stress concentrations consistent with central-core weakening under elevated head, providing a physically plausible interpretation of the remote-sensing evidence. Overall, integrating TW-PSI–densified InSAR with lightweight FEM discriminates plausible failure mechanisms and yields screening-level triggers for structural-health-monitoring prioritization in data-limited dam inventories, offering a scalable approach to dam-safety management.

Keywords: *ForensicSAR, SHM, InSAR, TW-PSI, Dam*

1. Introduction

Catastrophic dam failures can evolve with limited visible warning yet generate outsized impacts (A. A. Pratama & Takeuchi, 2024). The Derna disaster in Libya on 10–11 September 2023, in which two upstream embankment dams failed in cascade during Storm Daniel, has been reconstructed with rapid dam-break modelling and validation against multiple sources to recover timelines and plausible breach parameters in a data-limited setting (Annunziato et al., 2024). Comparative scenario analyses indicate that the downstream hazard was dominated by the event scale and cascading breach dynamics, highlighting limited mitigation at the highest intensities (Armon et al., 2025). Integrated hydrologic, hydraulic, and geotechnical studies formalized a four-phase internal response, saturation growth, overtopping and piping, subsequent deformation and deflection, and recent reanalysis argues that the hydrology likely falls within decadal return periods, implying uncertainty-aware risk design in drylands (Armon et al., 2025; Nemnem et al., 2025). Policy perspectives call for systematic safety audits, early-warning systems, and routine monitoring across

Libya's dam inventory (Cionek et al., 2019). Concurrently, InSAR time series has matured for dam forensics and early warning; before Brumadinho, ISBAS/SBAS revealed precursory deformation and enabled timing estimates (Grebby et al., 2021). Targeted DS/SIDS approaches densify sampling near seasonally inundated slopes and, with engineering forensics, localize vulnerable zones (Markogiannaki et al., 2022; Xie et al., 2025). These advances motivate integrating remote-sensing indicators with physics-based models for mechanism testing and screening-level decisions (Alegre et al., 2025; Sarayli et al., 2024; Wang et al., 2024). This study proposes ForensicSAR for Derna: we process Sentinel-1 LOS time series (January 2019–January 1, 2024), convert to vertical U and east–west E, and derive velocity, acceleration, and a two-segment $\Delta slope_{pre}$ over crest, faces, and abutments. To mitigate low coherence on dam bodies, we apply Tracy–Widom PS selection, increasing on-structure points by ~40% relative to ADI-PSI and stabilizing pre-event metrics. These satellite-derived constraints calibrate lightweight 2D plane-strain FEM sections to discriminate plausible failure mechanisms (seepage-induced softening, uplift pathways, shear localization), bridging retrospective forensics and prospective SHM.

2. Methodology

2.1 Study area and data

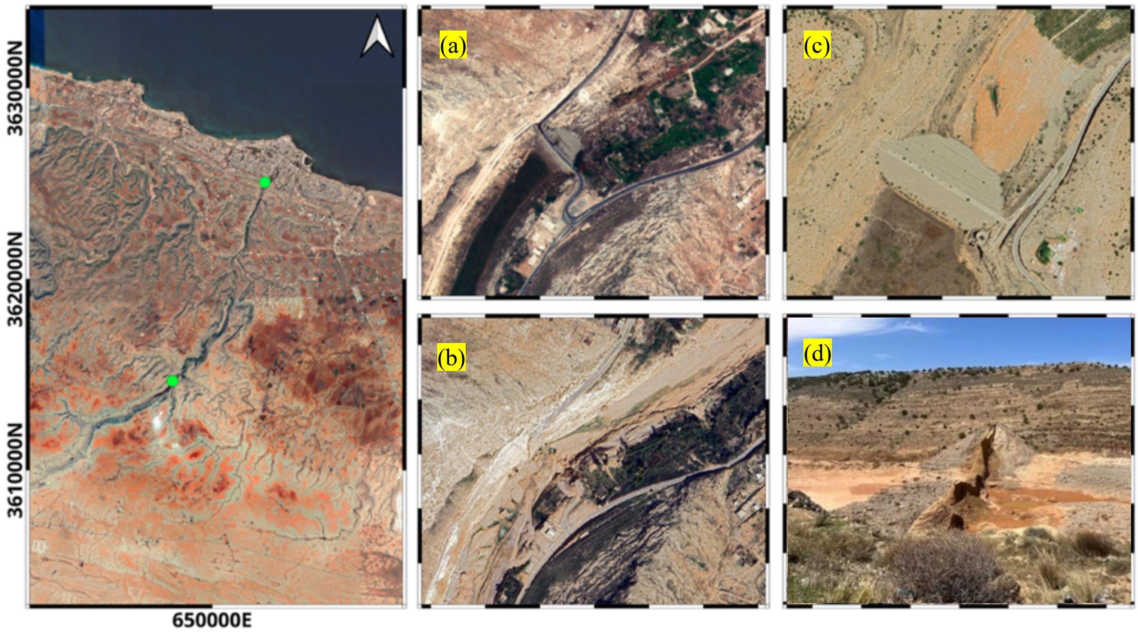

Figure 1. Study area. Green dots mark Al-Bilad (32.752° N, 22.630° E) and Bu Mansour (32.659° N, 22.577° E). Panels show Maxar pre- and post-event views of Al-Bilad (a, b), a pre-collapse view of Bu Mansour (c), and a post-collapse photograph of Bu Mansour (d).

Derna sits at the mouth of Wadi Derna, where two 1970s rockfill dams with clay cores regulate seasonal flow: Al-Bilad near the urban margin (downstream) and Bu Mansour farther upstream. Reconstructions of Storm Daniel (10–11 September 2023) indicate runoff far beyond combined storage and discharge capacity, with an upstream failure followed by a downstream breach that amplified flooding through the city (Annunziato et al., 2024; Nemnem et al., 2025). These studies show that event magnitude and cascading breach dynamics dominated the hazard, while maintenance and spillway adequacy remain central policy concerns (Armon et al., 2025; Cionek et al., 2019). We used Sentinel-1 Interferometric Wide acquisitions from January 2019 to January 2024, totaling 149 ascending and 151 descending VV scenes. Processing focused on the Al-Bilad and Bu Mansour structures and reservoirs. Dual-orbit coverage enabled conversion from Line-of-Sight (LOS) displacement to vertical and east–west components; SBAS provided domain-wide context, and TW-PSI delivered dense on-structure sampling to address low coherence over crest, faces, and abutments (Annunziato et al., 2024; Nemnem et al., 2025).

2.2 Enhanced InSAR and preliminary ForensicSAR

We form a small-baseline interferogram network and invert with SBAS to suppress decorrelation and isolate long-wavelength signals; phases comprise deformation, residual topography/DEM error, atmosphere, and noise (Yunjun et al., 2019). To densify on-structure sampling near crests/abutments, we add Tracy–Widom PS selection, testing each pixel's largest covariance eigenvalue against a robust threshold to retain subtle yet reliable scatterers that fixed coherence cutoffs miss (A. Pratama & Takeuchi, 2025):

$$\boldsymbol{\lambda_{max}} > \boldsymbol{\lambda_{TW}} = \text{Median}\,(\lambda) + \kappa \cdot \text{MAD} \cdot (\lambda) \tag{1}$$

Paired ascending/descending coverage converts LOS (positive toward satellite) to vertical U and east–west E components, from which we derive pre-event metrics (velocity, acceleration, two-segment $\Delta slope_{pre}$); in Derna, TW-PSI increased usable PS relative to ADI-PSI and stabilized trends. For mechanism screening, we calibrate lightweight 2D plane-strain Mohr–Coulomb models $(\rho, E, \nu, c, \phi, k)$ with hydrostatic head on the upstream slope and fixed foundation, minimizing a weighted sector-median misfit between modeled and observed U/E (weights σ_U, σ_E) while toggling simple scenario flags. Stability is reported via strength-reduction on $\tan\phi$ or an equivalent limit-analysis indicator, following practice for earth/tailings embankments (Sarayli et al., 2024; Whittle et al., 2022). Geometry and boundary conditions follow Derna reconstructions for the Al-Bilad–Bu Mansour system (Annunziato et al., 2024; Nemnem et al., 2025).

3. Results and Discussion

3.1 Enhanced point selection for InSAR time series

Figure 2 compares SBAS, ADI-PSI, and TW-PSI over the Derna corridor using descending-orbit LOS time series. SBAS provides broad context but yields few points on the dam bodies; ADI-PSI improves coverage at Al-Bilad and Bu Mansour**.** TW-PSI delivers the largest gains on the crest and abutments, enabling robust pre-collapse analysis. Quantitatively, TW-PSI identifies 484,040 PS versus 341,477 with ADI-PSI (~40% increase), reducing on-structure false negatives and stabilizing U and E metrics (velocity, acceleration, two-segment $\Delta\,slope_{pre}$). The denser sampling supplies constraints used in Section 3.3 to discriminate plausible failure mechanisms at Bu Mansour and supports screening-level triggers for dam safety in data-limited settings.

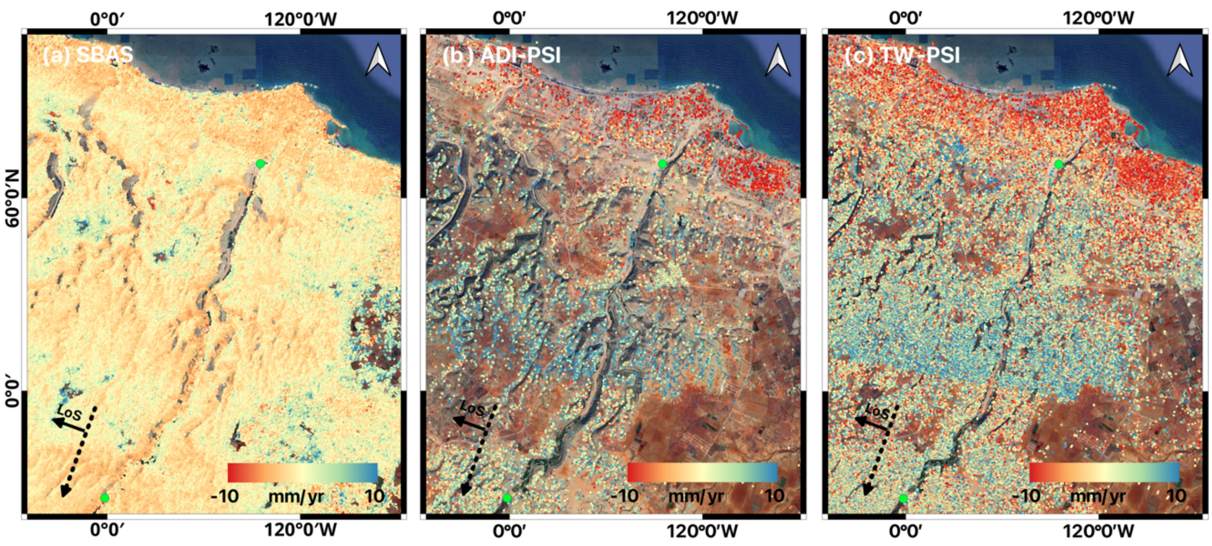

Figure 2. Point-selection comparison using descending-orbit LOS time series: (a) SBAS, (b) ADI-PSI, (c) TW-PSI. Green dots mark Al-Bilad and Bu Mansour.

3.2 Displacement over the dam structure

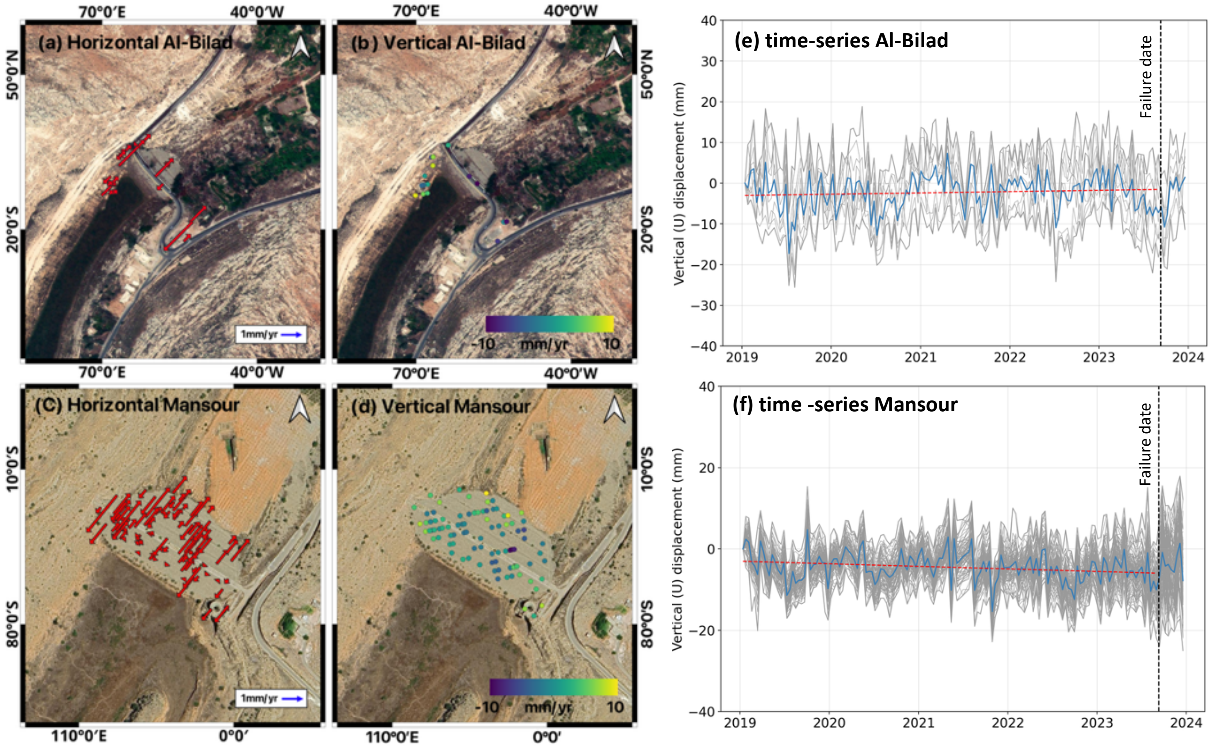

Figure 3. (a–b) Al-Bilad: horizontal (E) and vertical (U) components. (c–d) Bu Mansour: horizontal (E) and vertical (U). (e–f) Vertical U time-series for all persistent scatterers points (in the gray) with the mean in the blue, the red dashed line shows the pre-collapse trend.

Bu Mansour shows a clear, localized precursor. The vertical median shifts from −0.705 mm/yr at baseline to +0.780 mm/yr in the 12-month pre-event window, with a wide two-segment $\Delta slope_{pre}$ and a peak near −129.7 mm/yr ($z \approx 4.3$) on the eastern flank. The E component is small at baseline but exhibits an anomalous tail coherent with U; a projection along the upstream–downstream axis shows small sign changes consistent with flood-driven routing toward the city. Al-Bilad shows weaker, spatially diffuse precursors: pre-event medians trend downward without a focused $\Delta slope_{pre}$ cluster, consistent with hydrologic forcing rather than progressive geotechnical degradation detectable by InSAR. Table 1 mirrors these medians and ranges.

Table 1. Comparative deformation metrics (medians) for Bu Mansour and Al-Bilad. Velocities are in mm/yr; $\Delta slope_{pre}$ is the two-segment change in slope within the 12-month pre-event window.

	Component vertical (mm/yr)			**Component Horizontal (mm/yr)**		
	Baseline-Velocity	Pre-event Velocity	(Δ))Slope Pre-event	Baseline-Velocity	Pre-event Velocity	(Δ))Slope Pre-event
Bu Mansour	-0.705	0.780	-196.0 to -56.8	0.128	-1.000	-139.6 to 119.9
Al-Bilad	0.395	-6.976	-223.1 to 200.5	-0.387	-2.296	-387.8 to 296.3

3.3 Displacement over the dam structure

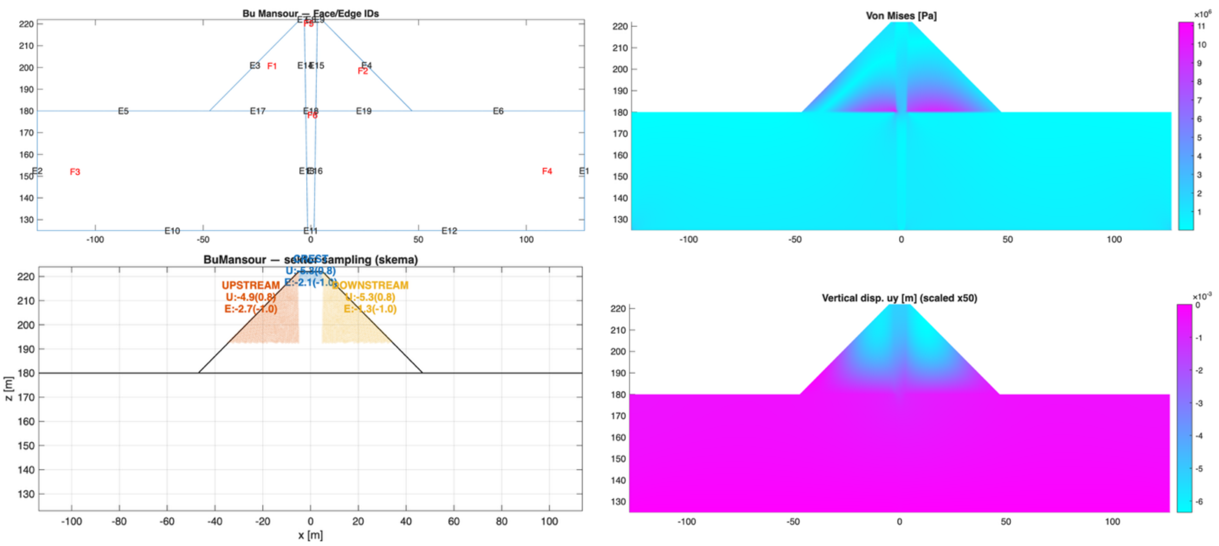

Figure 4. Deformation and stress response at reservoir elevation 222 m (datum X). Hydrostatic pressure is applied as $p = \rho g h$ using local water depth h along the upstream face; results are consistent with a central-core-weakening scenario.

At reservoir elevation 222 m, we impose hydrostatic loading $p = \rho g h$ on the upstream face with a fixed foundation. In the core-cracked scenario, the vertical displacement map u_z shows crest-focused settlement of ~5–6 mm, decaying toward the shoulders and approaching zero in the foundation, which is typical of a compressible core under high head. The von Mises equivalent stress σ_{vm} concentrates along the core faces (near the rockfill interface ~180 m elevation and beneath the crest), consistent with internal shear localization after integrity loss. A strength-reduction run reports FoS ≈ 0.10; we treat this strictly as a screening indicator, not a definitive stability measure. Crucially, calibration uses sector-level U/E metrics from TW-PSI-densified InSAR, supplying quantitative deformation targets and enabling mechanism discrimination. The combined evidence, including crest settlement, core focused stress, and agreement with InSAR trends, supports a central core weakening pathway and provides screening level triggers for dam safety management in data limited settings.

4. Conclusion

Tracy–Widom PS selection increased on-structure persistent scatterers by about 40% (484,040 versus 341,477), enabling stable conversion from LOS to vertical $U$and east–west Etime series and reliable pre-event metrics. Bu Mansour exhibits a focused precursor: the vertical median shifts from −0.705 mm/yr to +0.780 mm/yr in the final 12 months with a wide $\Delta\text{slope}_{\text{pre}}$ range (−196.0 to −56.8 mm/yr) and an Etail coherent with U. Al-Bilad shows downward pre-event medians ($U = -6.976$ mm/yr) without a concentrated $\Delta\,\text{slope}_{\text{pre}}$ cluster, indicating hydrologic forcing rather than progressive geotechnical degradation detectable by InSAR. Plane-strain FEM under high head reproduces crest settlement and core-face stress concentration at Bu Mansour, consistent with a cracked and softening core, while Al-Bilad remains largely hydrologically driven. Together, these results demonstrate that ForensicSAR can prioritize assets, calibrate structural health-monitoring models, and provide screening level triggers where ground observations are limited.

References

Alegre, A., Oliveira, S., Proença, J., Mendes, P., & Carvalho, E. (2025). A Finite Element Formulation for True Coupled Modal Analysis and Nonlinear Seismic Modeling of Dam–Reservoir–Foundation Systems: Application to an Arch Dam and Validation. *Infrastructures*, *10*(8), 193. https://doi.org/10.3390/infrastructures10080193

Annunziato, A., Santini, M., Proietti, C., de Girolamo, L., Lorini, V., Gerhardinger, A., & Tucci, M. (2024). Modelling and Validation of the Derna Dam Break Event. *GeoHazards*, *5*(2), 504–529. https://doi.org/10.3390/geohazards5020026

Armon, M., Shmilovitz, Y., & Dente, E. (2025). Anatomy of a foreseeable disaster: Lessons from the 2023 dam-breaching flood in Derna, Libya. In *Sci. Adv* (Vol. 11). https://www.science.org

Cionek, V. M., Zaia Alves, G. H., Tófoli, R. M., Rodrigues-Filho, J. L., & Dias, R. M. (2019). Brazil in the mud again: lessons not learned from Mariana dam collapse. In *Biodiversity and Conservation* (Vol. 28, Issue 7, pp. 1935–1938). Springer Science and Business Media B.V. https://doi.org/10.1007/s10531-019-01762-3

Grebby, S., Sowter, A., Gluyas, J., Toll, D., Gee, D., Athab, A., & Girindran, R. (2021). Advanced analysis of satellite data reveals ground deformation precursors to the Brumadinho Tailings Dam collapse. *Communications Earth and Environment*, *2*(1). https://doi.org/10.1038/s43247-020-00079-2

Markogiannaki, O., Xu, H., Chen, F., Mitoulis, S. A., & Parcharidis, I. (2022). Monitoring of a landmark bridge using SAR interferometry coupled with engineering data and forensics. *International Journal of Remote Sensing*, *43*(1), 95–119. https://doi.org/10.1080/01431161.2021.2003468

Nemnem, A. M., Tanim, A. H., Nahian, A., Khan, S., Goharian, E., & Imran, J. (2025). How extreme rainfall and failing dams unleashed the Derna flood disaster. *Nature Communications* , *16*(1). https://doi.org/10.1038/s41467-025-59261-9

Pratama, A. A., & Takeuchi, W. (2024). DETECTION OF MILLIMETER-SCALE DEFORMATIONS AT JATILUHUR DAM USING PERSISTENT SCATTERER INSAR (PS-INSAR). *PLANTATION STUDIES Volume*, 141.

Pratama, A., & Takeuchi, W. (2025). Investigating structural health of rock earth-filled Jatiluhur Dam after a shallow earthquake using multi-technique InSAR time-series. *Proceedings of the IEEE International Geoscience and Remote Sensing Symposium (IGARSS)*.

Sarayli, S., Sert, S., & Sonmez, O. (2024). Analysis of Fill Dam Using Finite Element Method and Comparison with Monitoring Results. *Water (Switzerland)*, *16*(17). https://doi.org/10.3390/w16172387

Wang, Y., Liu, F., Kou, M., & Li, M. (2024). A Review of Stability of Dam Structures in Coal Mine Underground Reservoirs. In *Water (Switzerland)* (Vol. 16, Issue 13). Multidisciplinary Digital Publishing Institute (MDPI). https://doi.org/10.3390/w16131856

Whittle, A. J., El-Naggar, H. M., Akl, S. A. Y., & Galaa, A. M. (2022). Stability Analysis of Upstream Tailings Dam Using Numerical Limit Analyses. *Journal of Geotechnical and Geoenvironmental Engineering*, *148*(6). https://doi.org/10.1061/(asce)gt.1943-5606.0002792

Xie, L., Xu, W., & Aoki, Y. (2025). Extracting a decadal deformation on Xiaolangdi upstream dam slope using seasonally inundated distributed scatterers InSAR (SIDS − InSAR). *International Journal of Applied Earth Observation and Geoinformation*, *138*. https://doi.org/10.1016/j.jag.2025.104462

Yunjun, Z., Fattahi, H., & Amelung, F. (2019). Small baseline InSAR time series analysis: Unwrapping error correction and noise reduction. *Computers & Geosciences*, *133*, 104331.

Photo of post-collapse Bu Mansour. International Crisis Group. (2023, October 2). *When the dams in Libya burst: A natural or preventable disaster?* https://www.crisisgroup.org/middle-east-north-africa/north-africa/libya/when-dams-libya-burst-natural-or-preventable-disaster